Computation of a free jet with embedded drops

Kausik Sarkar*, William R. Schowalter

Department of Chemical Engineering, University of Illinois at Urbana-Champaign, Urbana, IL 61801, USA

Abstract

An inertialess jet containing Newtonian drops in a gravitation-free field has been modeled by incorporating the detailed micro-structural dynamics. Interactions of the drops with the continuous phase, with the wall, and with the jet surface are accounted for, thereby eliminating the need for additional constitutive assumptions. The deformation of the jet and drops, and the dispersion of drops are predicted. The present paper serves two purposes. First, a complete description of the modeling process and its limitation is presented. Second, preliminary results for single and for small clusters of drops indicate the potential inherent in this computational approach. The model flow is solved in two dimensions using the boundary element method (BEM). Effects of different drop parameters, such as their number, relative position, and interfacial tension are investigated. © 2002 Published by Elsevier Science B.V.

Keywords: Drops; BEM; Jet; Emulsion; Die-swell

1. Introduction

Expansion of a low Reynolds number jet upon exiting from a conduit is commonly known as die-, or extrudate-swell. It occurs due to the gradual relaxation of the parabolic flow inside the jet to a plug flow far downstream. The swelling is particularly pronounced in the case of elastic fluids, such as polymer melts, molten glass or metal or food paste, and therefore, is of utmost importance to processing and manufacturing industries. However, even a Newtonian jet experiences modest swelling, as was observed by Middleman and Gavis [1]. The phenomenon has been the subject of extensive theoretical (e.g. [2–7]) and numerical (e.g. [8–16]) investigations.

The present effort was inspired by an experimental observation of Ouddiz [17] (see also [18]) showing that an emulsion jet issuing into an immiscible medium undergoes considerable swelling, and the subsequent realization that the microstructure of this flow is governed by Newtonian fluid mechanics. As a motivation for studying particulate flows, Batchelor noted that such flows provide ideal non-Newtonian

scenarios where the governing equations (Stokes flow of Newtonian fluid) for the microstructural dynamics are readily available [19]. Therefore, one does not require any constitutive modeling, which in itself is a formidable task. Furthermore, these flows are experimentally realizable systems, displaying most of the non-Newtonian behavior commonly seen in polymer flows. In the case of emulsions, the tension at the drop interface readily provides a source of bulk elasticity. Nonisotropic microstructure generated by deformed drops leads to normal stresses, and nonlinearity in the stress is naturally built into the interacting interface dynamics. In fact, emulsions can be a realistic model for immiscible polymer blends, and have been applied as such. Finally, their ubiquitous presence in chemical and petroleum industries amply demonstrates the importance of two-phase flows of Newtonian fluids.

As indicated, die-swell has a long and illustrious history of investigation, and is a rich source of fundamental fluid mechanics issues, many yet to be satisfactorily resolved. For instance, the abrupt change in boundary condition at the lip leads to the classical stick-slip problem. The small-parameter perturbation analysis of this problem was pioneered by Richardson, who applied the Wiener–Hopf technique [3,4]. Such analytical treatments are notoriously difficult because of the nonlinear boundary condition on the free surface. Notable analyses are those by Trogden and Joseph for viscous flows with both small and large surface tensions [5,6], and by Sturges [7] for second-order viscoelastic flows. Early finite element simulation of this phenomenon was attempted by Nickell et al. [8], and then continued by several researchers [14–16]. Recently, application of special elements near the jet-lip that embody the form of the singularity in the local stress field has been advocated for performance improvement of finite element analysis [14]. Salamon et al. have performed a detailed finite element study of the planar jet using high resolution quadrilateral isoparametric elements with quasi-orthogonal mesh generation [15]. Their investigation includes validation of the nature of the singularity and the curvature of the free surface suggested in [14], effects of Reynolds number and capillary number variations, as well as the Navier type slip condition proposed earlier by Silliman and Scriven [20]. Finite element investigation has been extended to viscoelastic fluids governed by simple rheological models such as the upper convected Maxwell (e.g. [9]), including some recent modeling of complex three-dimensional die shapes [16].

Bush and Tanner [10] initiated the boundary element investigation of the problem, which has been subsequently extended to viscoelastic fluids governed by a number of constitutive models [12,13]. Here we have adopted the boundary element method primarily because it is well suited to handle the moving boundary problem (i.e. both jet and drops). It implements an integral equation formulation for Newtonian–Stokes flow involving unknowns only on the boundary, and thereby effectively reduces the spatial dimension of the problem by one. In the case of viscoelastic constitutive equations or flows with inertia, one must deal with additional volume terms that require further discretization [12,13]. We note that Youngren and Acrivos have pioneered the use of boundary integral methods for Stokes flow a quarter of a century ago [21,22], and made seminal contributions to the field of emulsions.

There is an extensive literature on boundary element solution of single or multiple drop deformation and breakup [23–25], as well as those at finite Reynolds number [26–28]. In this paper, we provide the mathematical model for the jet emulsion in some detail, briefly delineate the numerical method, and present some preliminary computations in two dimensions with a small number of drops dispersed in a jet. The two-dimensionality admittedly restricts the quantitative applicability of our results to any real problem. However, we believe the formidable difficulty of the problem justifies the present simpler effort, which has provided valuable insights for future three-dimensional studies. We note that most of the qualitative understandings are readily transferable to three dimensions. Also, although the present results are limited to low concentrations of the dispersed phase, new applications come to mind. For

example, there are processes involving microfluidic patterning or control where the shape of embedded drops exiting from a nozzle can be important.

2. Mathematical formulation

2.1. Governing equations

Fig. 1 describes the geometry of the flow under investigation. The flow field (that is velocity u_i and pressure p) is assumed to satisfy Stokes equation:

$$-\partial_i p + \mu \nabla^2 u_i = 0, \qquad \partial_i u_i = 0. \tag{2.1}$$

Inside a drop the same equations hold with viscosity μ replaced by μ^α, $\alpha = 1, \ldots, N$, where N is the number of drops. Across the surface $\partial\Omega^\alpha$ of the α-th drop velocity and tangential traction are assumed to be continuous. However, the normal stress satisfies the appropriate jump condition:

$$n_i(p_{ij} - p_{ij}^\alpha)n_j = \sigma^\alpha \mathcal{C}, \tag{2.2}$$

where $\mathcal{C}$ is the curvature of the interface, and σ^α the interfacial tension. The stress tensor p_{ij} follows the Newtonian constitutive law

$$p_{ij} = -p\delta_{ij} + 2\mu e_{ij}, \qquad e_{ij} = \tfrac{1}{2}(\partial_i u_j + \partial_j u_i). \tag{2.3}$$

At the rigid wall $\partial\Omega^w$, a no-slip condition is imposed. The drop shape is governed by the kinematic condition

$$\frac{dx_i}{dt} = u_i, \tag{2.4}$$

for a material point $x \in \partial\Omega^\alpha$. The jet issues from the rigid enclosure $\partial\Omega^w$, and expands in free space, where the jet surface is denoted by $\partial\Omega^f$. Its evolution is described by an equation identical to Eq. (2.4) for $x \in \partial\Omega^f$. The tangential component of the traction is zero at $\partial\Omega^f$, and the normal component has a jump across the surface:

$$p_{ij}n_j = n_i\sigma\mathcal{C}, \tag{2.5}$$

σ being the surface tension at the free surface.
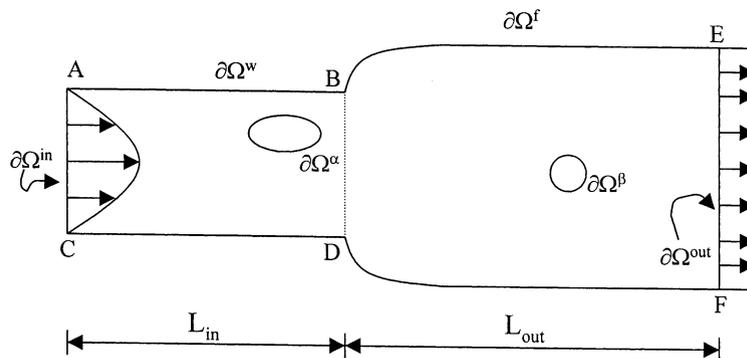
Fig. 1. Jet geometry.

We nondimensionalize the equations with velocity scale U_0 (e.g. the center-line velocity at $\partial \Omega^{\text{in}}$) and the conduit half-width R. Pressure and stresses are nondimensionalized by $\mu U_0/R$ to arrive at the following:

$$-\partial_i p + \nabla^2 u_i = 0, \qquad -\partial_i p + \lambda^\alpha \nabla^2 u_i = 0 \text{ inside } \alpha\text{-th drop}, \tag{2.6}$$

where $\lambda^\alpha = \mu^\alpha/\mu$. The incompressibility and the kinematic evolution (2.4) remain the same after nondimensionalization. However, the normal traction conditions (2.2) and (2.5) become

$$n_i(p_{ij} - p_{ij}^\alpha)n_j = k^\alpha \mathcal{C}, \tag{2.7}$$

and

$$p_{ij}n_j = n_i k \mathcal{C}, \tag{2.8}$$

where $k = \sigma/(U_0\mu)$ and $k^\alpha = \sigma^\alpha/(U_0\mu)$ are inverse of capillary numbers at the free and drop surfaces, respectively. The computational domain Ω is further bounded by a prescribed inlet boundary $\partial \Omega^{\text{in}}$ sufficiently far upstream from the conduit exit so that a fully developed parabolic flow can be assumed. Far downstream from the exit, an outlet boundary $\partial \Omega^{\text{out}}$ is provided. The jet is, therefore, inscribed by $\partial \Omega = \partial \Omega^{\text{in}} \cup \partial \Omega^{\text{w}} \cup \partial \Omega^f \cup \partial \Omega^{\text{out}}$.

We briefly describe the boundary integral method [23] applied here. Using the reciprocal theorem for Stokes flow, one can obtain an expression for the velocity as follows:

$$c_{ij}u_i(x_0) = -\int_{\partial \Omega} f_i(x)G_{ij}(x, x_0)\, dl(x) + \int_{\partial \Omega} u_i(x)T_{ijk}(x, x_0)n_k(x)\, dl(x), \tag{2.9}$$

where

$$G_{ij}(x, x_0) = -\delta_{ij} \ln |x - x_0| + \frac{(x - x_0)_i(x - x_0)_j}{|x - x_0|^2},$$

$$T_{ijk}(x, x_0) = -4\frac{(x - x_0)_i(x - x_0)_j(x - x_0)_k}{|x - x_0|^4}, \tag{2.10}$$

where n is the inward normal to the boundary, and $f_i = p_{ij}n_j$ is the traction; $c_{ij} = 4\pi\delta_{ij}$ inside the domain; $2\pi\delta_{ij}$ on a smooth part of the boundary, and zero outside. We note that for a point on the non-smooth part of the boundary (such as points A, B or E in Fig. 1), c_{ij} is not diagonal, but could be computed by an integral involving T_{ijk} similar to the one in Eq. (2.9). The discretization scheme adopted here (see the following paragraphs) does not require computation of c_{ij} at such points. With drops embedded in the jet, we consider the domain of the continuous medium bounded by them, and the boundary is modified: $\partial \overline{\Omega} = \partial \Omega \cup \sum_{\alpha=1}^N \partial \Omega^\alpha$. Note that the normal to the drop surface points inward to the domain, i.e. outward on the drop surface. Similarly for flow inside the α-th drop, one can write:

$$\lambda^\alpha c_{ij}^\alpha u_i^*(x_0) = -\int_{\partial \Omega^\alpha} f_i^*(x)G_{ij}(x, x_0)\, dl(x) + \lambda^\alpha \int_{\partial \Omega^\alpha} u_i^*(x)T_{ijk}(x, x_0)n_k^*(x)\, dl(x), \tag{2.11}$$

where $n^* = -n$ is the normal inward to the drop surface. The asterisk indicates that the variable is defined for the domain inside the drop. We add modified Eq. (2.9) (with the effects of the drops, i.e. $\partial \Omega$ replaced

by $\partial\overline{\Omega}$) to Eq. (2.11) for each drop, and obtain the following:

$$[c_{ij} + \lambda^\alpha c_{ij}^\alpha]u_i(x_0) = -\int_{\partial\Omega} f_i(x)G_{ij}(x, x_0)\,\mathrm{d}l(x) + \int_{\partial\Omega} u_i(x)T_{ijk}(x, x_0)n_k(x)\,\mathrm{d}l(x)$$

$$-\sum_{\alpha=1}^N \int_{\partial\Omega^\alpha} \Delta f_i(x)G_{ij}(x, x_0)\,\mathrm{d}l(x)$$

$$+\sum_{\alpha=1}^N (1-\lambda^\alpha) \int_{\partial\Omega^\alpha} u_i(x)T_{ijk}(x, x_0)n_k(x)\,\mathrm{d}l(x). \tag{2.12}$$

Note that we have used velocity continuity $u^*(x) = u(x)$ for $x \in \partial\Omega^\alpha$ and

$$\Delta f_i = k^\alpha \mathcal{C}n_i. \tag{2.13}$$

Also note that $\lambda^\alpha = 1$ removes velocity at the α-th drop surface from inside the integral. This is a well-known condition for viscosity-matched multiphase boundary element method (BEM) problems, where the unknowns at the internal surface do not appear explicitly in the equation, and therefore, need not be explicitly solved at the outset. One can obtain them afterwards by solving for the unknown forces and velocities at the external surface. For simplicity, all the results presented here are for $\lambda^\alpha = 1$.

2.2. Computational aspects

For computational purposes the inlet and the outlet boundaries $\partial\Omega^{\mathrm{in}}$ and $\partial\Omega^{\mathrm{out}}$ are placed at finite distances, L^{in} and L^{out} respectively from the conduit exit (Fig. 1). At the inlet, we assume fully developed parabolic profile (nondimensionalized by center line velocity U_0)

$$u(x_1 = -L^{\mathrm{in}}) = (1 - x_2^2); \qquad f_i(x_1 = -L^{\mathrm{in}}) = -p^{\mathrm{in}}\delta_{i1} - 2x_2\delta_{i2}. \tag{2.14}$$

Note that the inlet pressure p^{in}, assumed to be laterally uniform, is not known, and has to be solved along with other variables. At $\partial\Omega^{\mathrm{out}}$ a zero stress condition is imposed, which is equivalent to a fully developed plane plug flow. One can alternatively impose velocity conditions (constant u_1 and zero u_2). However, the zero stress condition seems to be a better option for numerical implementation (see the following paragraphs).

We discretize all boundaries by inserting points, and interpolate the unknowns as constants over elements. The integration is performed with 16 Gauss quadrature points per element. The singularities in the integrand when $x_0 \to x$ are analytically accounted for (see Appendix B). The drop and the free surfaces are described by cubic splines. The inlet $\partial\Omega^{\mathrm{in}}$ is represented by only one element, and the outlet $\partial\Omega^{\mathrm{out}}$ by four. After performing the integrals, we obtain a linear set of equations for the unknowns, which in the present case are the inlet pressure p^{in}, the force vectors f_i^s on the rigid surface $\partial\Omega^{\mathrm{w}}$, and the velocity vectors u_i^s at the moving surfaces, jet ($\partial\Omega^f$), drops ($\partial\Omega^\alpha$; $\alpha = 1, \ldots, N$), and the outlet boundary $\partial\Omega^{\mathrm{out}}$:

$$-\overline{\mathcal{A}}_j^{r;\mathrm{in}} p^{\mathrm{in}} - \sum_{s;\mathrm{wall}} \mathcal{A}_{ij}^{rs} f_i^s + \sum_{s;\mathrm{free}} \mathcal{B}_{ij}^{rs} u_i^s + \sum_{s;\mathrm{out}} \mathcal{B}_{ij}^{rs} u_i^s + \sum_{\alpha=1}^N \sum_{s;\partial\Omega^\alpha} (1-\lambda^\alpha)\mathcal{B}_{ij}^{rs} u_i^s - [c_{ij}^r + \lambda c_{ij}^{r\alpha}]u_i^r$$

$$= \mathcal{A}_j^{r;\mathrm{in}} - \mathcal{B}_j^{r;\mathrm{in}} + k\mathcal{A}_j^{r;\mathrm{free}} + \sum_{\alpha=1}^N k^\alpha \mathcal{A}_j^{r;\alpha}, \tag{2.15}$$
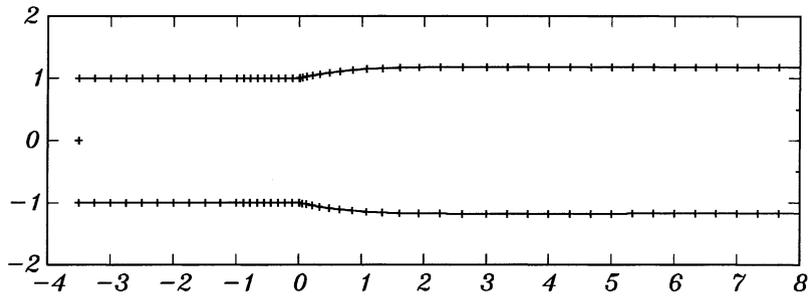
Fig. 2. The steady single phase jet with the discretization of the boundary.

where $\mathcal{A}$ refers to integrals containing G_{ij}, and $\mathcal{B}$ to those containing T_{ijk}. The right-hand side of the above equations contains known quantities. Explicit expressions for these quantities are obtained in Appendix A. The indices r and s are not summed on repetition; r corresponds to the boundary point x_0 where the velocity is being determined, and s to the boundary points arising from the surface integrals.

2.3. Algorithm

At the outset, we use an iterative process to solve for the shape of the steady, single-phase jet without drops (Bush et al. [12]). Initially an undeformed straight, free surface is assumed. The set of Eq. (2.15)
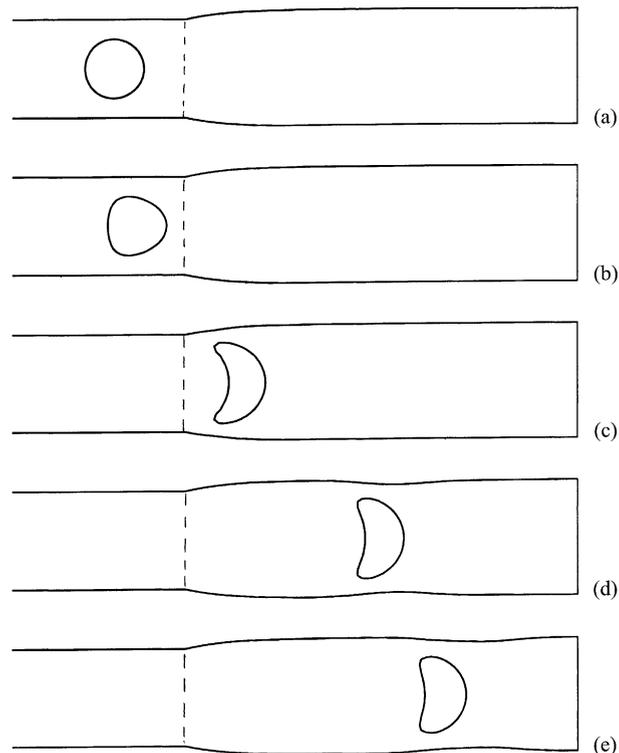
Fig. 3. Time-shots at (a) $t = 0.09$, (b) $t = 0.79$, (c) $t = 5.06$, (d) $t = 12.47$, (e) $t = 15.77$, for $k^1 = 0.1$ and $a = 0.6$.

without the drop terms (those involving α) is solved for the velocity at the nodes on the jet surface. The elements on the free surface are reoriented to align them along the streamline defined by the computed velocity, starting from the first element at the conduit exit (points B and D). The integrals are recomputed with the new shape to arrive at a new set of coefficients in Eq. (2.15). The process is iterated until a converged, steady jet is achieved.

The undeformed drops are then introduced inside the jet. Eq. (2.15) is solved to find velocities both on the drop and the jet surfaces. The computed velocity at the element center is interpolated to the element nodes, and their new positions are determined using Eq. (2.4). An Euler scheme is applied for the time integration. Due to the explicit nature of the scheme, the time stepping is limited by numerical capillary instability $\Delta t < \Delta x / (U_{max} k_{max})$. The nodes on the drop surface are periodically redistributed to achieve equal-size elements.

Several brief comments are in order. The initial drop shapes are assumed to be circular on the premise that given a long enough inlet region L^{in}, drops will achieve equilibrium shapes corresponding to a steady pipe flow before reaching the conduit exit. This may or may not be the case, and depending on the parameter values, one may need different computation lengths. However, note that the method allows considerable flexibility in the initial positions and shape of drops. Also, the pressure is assumed to be laterally uniform across the width, which could easily be relaxed by introducing more nodes along $\partial\Omega^{in}$, and would be more appropriate in case fully developed flow is not present there. The other limitation is at the outlet $\partial\Omega^{out}$. Note that the jet width is not known a priori there. In reality it will vary in response
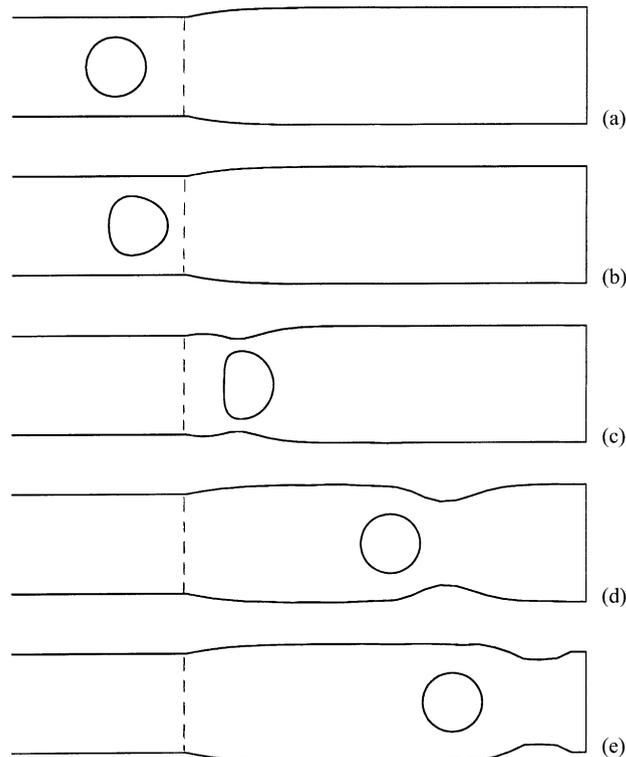
Fig. 4. Time-shots at (a) $t = 0.09$, (b) $t = 0.79$, (c) $t = 5.06$, (d) $t = 12.47$, (e) $t = 15.77$, for $k^1 = 1.0$ and $a = 0.6$.

to drop motion. However, here it is fixed at the single-phase steady state value at the outset. Even with the stress (as opposed to a velocity) condition, outlet width cannot vary, and would inhibit the free surface deformation at the outlet. The traction-free boundary condition imposed at $\partial \Omega^{\text{out}}$ indicates a fully developed plane plug flow. The axial velocity at $\partial \Omega^{\text{out}}$ can change with time because the jet geometry $\partial \Omega^{f}$ is influenced by the time dependent shape and location of the drops. However, the vertical velocity is stated to be zero at the vertices E and F (Fig. 1). Note that this condition is not exactly matched because a constant interpolation scheme has been used. The present model is not realistic when the drops are close to the outlet, which requires a large lateral deformation of the jet. These small discrepancies are believed to be unimportant when the drops are far from $\partial \Omega^{\text{out}}$.

3. Numerical Results

As mentioned before, the jet is computationally defined by a finite domain. In this paper, we use $L^{\text{in}} = 3.5$ and $L^{\text{out}} = 8.0$ except when stated otherwise (the cases with five drops below). The rigid part of the wall $\partial \Omega^{\text{w}}$ is discretized with 20 nodes, $\partial \Omega^{f}$ with 30 nodes, and drops with 40 nodes each. In this article, calculations have been restricted to the case of $\sigma = 0$ ($k = 0$) at the jet surface. We experienced convergence problems in our algorithm for shape of a single-phase jet at nonzero surface
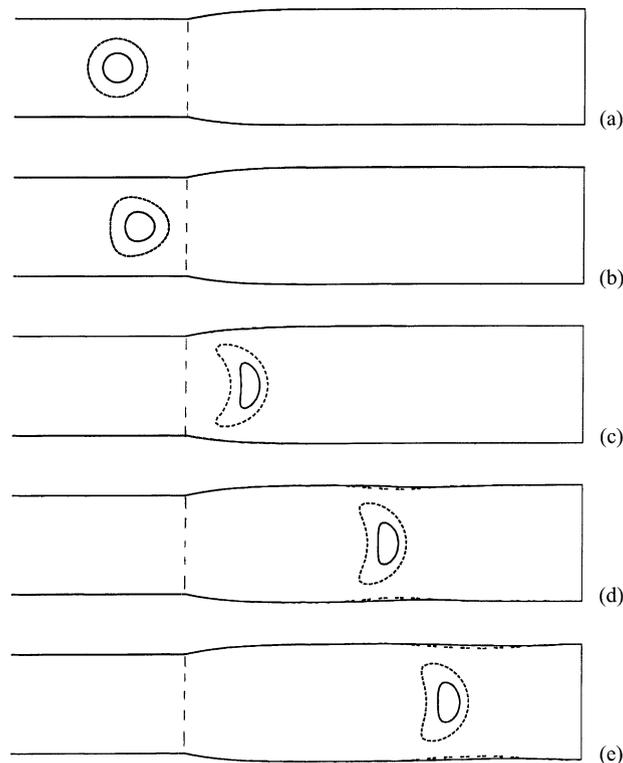
Fig. 5. Time-shots at (a) $t = 0.09$, (b) $t = 0.79$, (c) $t = 5.06$, (d) $t = 12.47$, (e) $t = 15.77$, for $k^{1} = 0.05$ and $a = 0.3$, overlayed on time-shots (dotted line) at the same time instants for $k^{1} = 0.1$ and $a = 0.6$ from Fig. 3.
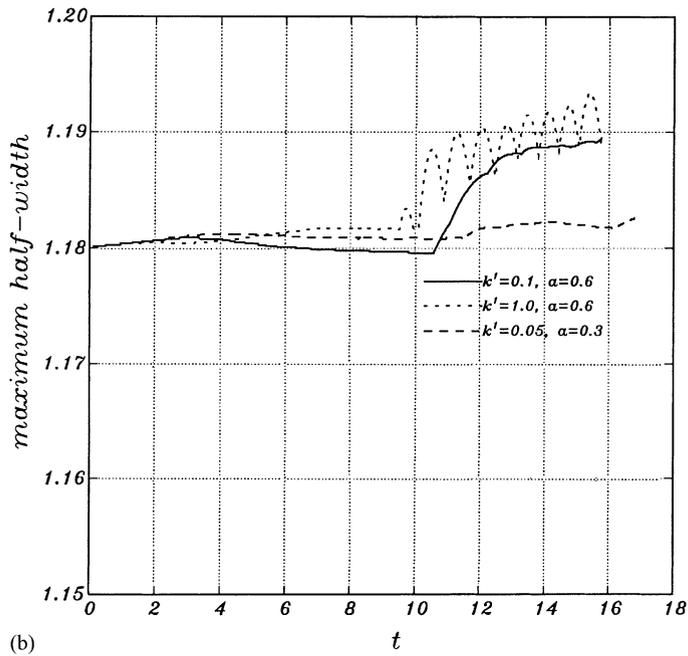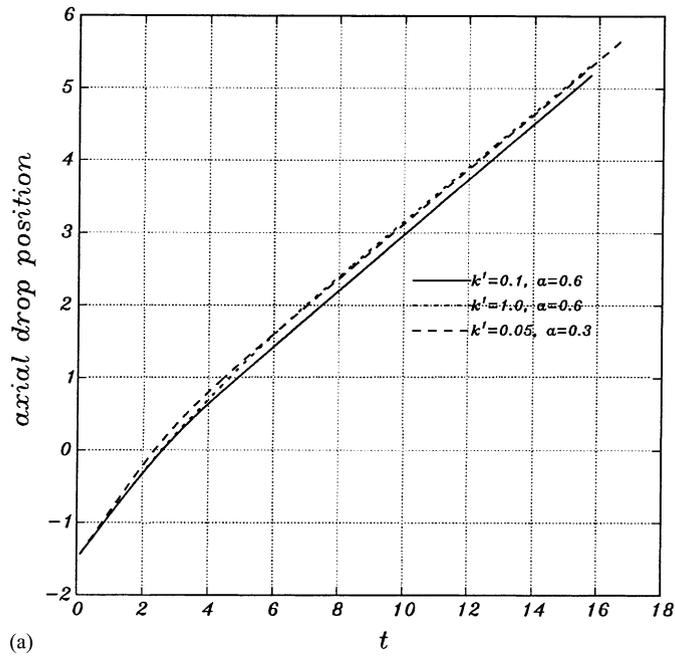
Fig. 6. (a) Axial drop position, and (b) maximum lateral extent of the jet as functions of time.

tensions. This result is possibly related to an observation by Silliman and Scriven [20]. They found iteration on a kinematic boundary condition at the outlet to be the most effective at $k \ll 1$, while a normal stress condition was superior at $k \gg 1$. For zero surface tension, we recovered the result (Fig. 2) of [14] which is a diameter expansion of $\sim$18% (note that at the drop surface, tension is nonzero). For nonzero k, one requires an under-relaxation in the iteration scheme for jet shape determination.

We introduce a drop of radius $a = 0.6$ along the center-line of the jet at an axial distance $x_0 = -1.5$ (measured from the conduit exit). The rather large drop can also act as a model of a cluster of small drops. Fig. 3 shows the jet and the drop geometry at five different time instants. The drop is first deformed by the steady, wall-bounded planar parabolic flow. However, as the drop emerges from the enclosure, it slowly relaxes as is obvious from the last three time-shots. The jet surface is markedly influenced by the drop dynamics. We increase the interfacial tension to $k^1 = 1.0$ in Fig. 4, for which we would expect far more effects on the free surface. And indeed for the same last three time instants shown in Fig. 3, the shapes for this case are significantly different. Increased tension leads to a quicker relaxation of the drop shape, and a region of increased jet deformation is seen trailing behind the relaxing drop, with a compensating dip in front. As has been noted before, the tension at the drop interface serves the same purpose as bulk elasticity, and therefore, leads to larger swelling. Also, note that the effects of the outlet conditions influence the last time-shot. One would have to increase the length of the computed jet to obtain realistic data at such a later time instant. Fig. 5 indicates the effect of drop radius. We introduce a drop of radius $a = 0.3$,
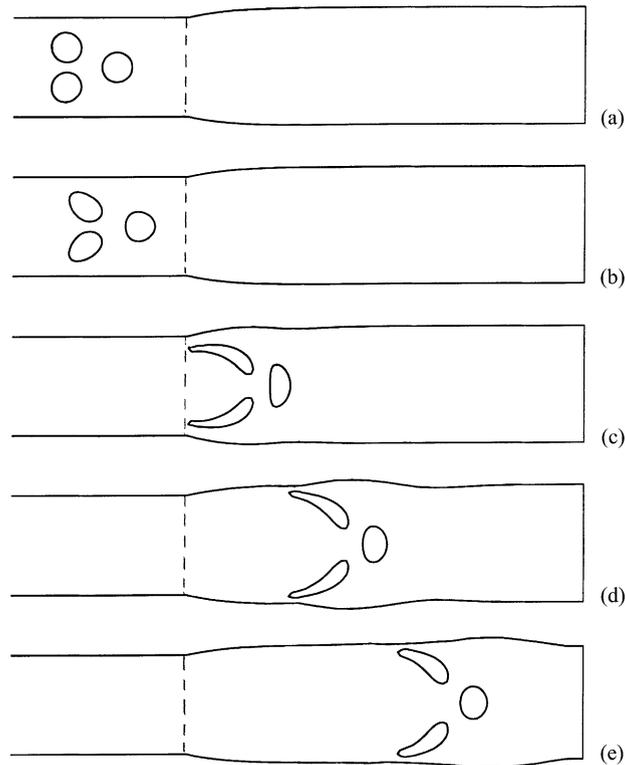
Fig. 7. Time-shots at (a) $t = 0.1$, (b) $t = 0.82$, (c) $t = 6.72$, (d) $t = 12.15$, (e) $t = 17.73$, for $k^1 = 0.1$ and $a = 0.3$ for all drops.

but $k^1 = 0.05$ to keep $k^1/a = 0.167$ the same as that for Fig. 3. Note that k^1/a is the capillary number inverse based on the drop radius rather than the conduit half-width R. The time-shots at the same time instants are overlayed on those from Fig. 3. The smaller radius leads to a decreased drop deformation, and a quicker relaxation. The effects on the jet surface are similar. In Fig. 6, we plot the drop position, and the maximum lateral extent of the jet at any point along its boundary as a function of time for these three different simulations. The position of a drop is determined by finding moments of the drop interface:

$$x_i^\alpha = \frac{\int_{\partial \Omega^\alpha} x_i \, dl}{\int_{\partial \Omega^\alpha} dl}, \quad i = 1, 2. \tag{3.1}$$

Unlike the integrals used earlier, a simple trapezoidal rule is used over linear elements described by the nodes. The drops have very similar speed except for the large drop ($a = 0.6$) with $k^1 = 0.1$. Because of its excessive backward deformation (Fig. 3) the drop with $k^1 = 0.1, a = 0.6$ tends to lag. It is seen that the jet experiences small additional swelling as the drop passes. The oscillating part of the curve for $k^1 = 1.0, a = 0.6$ is due to surface discretization; the maximum shifts from one node to the next as time progresses. The oscillation magnitude should be taken as an error bar for the actual physical value. We see that the increased value of k^1 leads to an increased swelling. However, for the smaller drop, it seems that as the drop is completely relaxed, the jet surface partially shrinks back. One should finally keep in mind that the actual value of the effect is quite small.
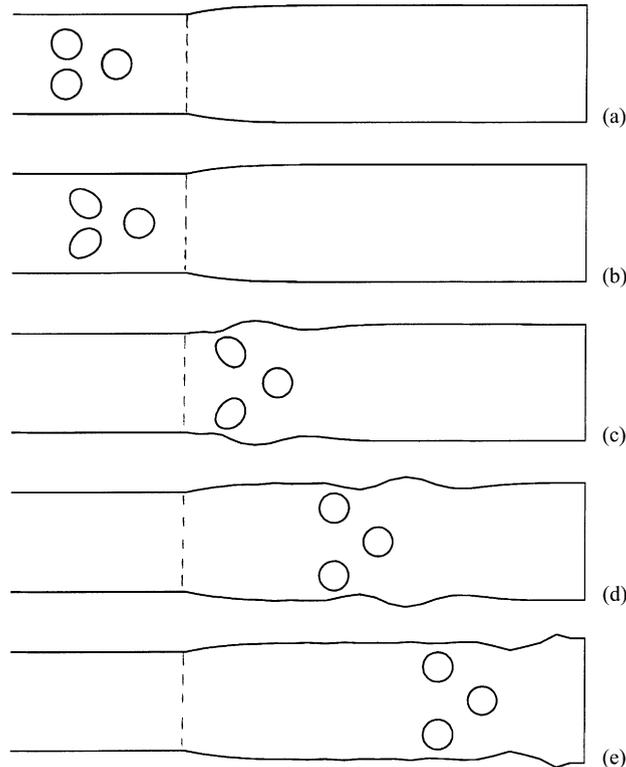
Fig. 8. Time-shots at (a) $t = 0.1$, (b) $t = 0.82$, (c) $t = 6.72$, (d) $t = 12.15$, (e) $t = 17.73$, for $k^1 = 1.0$ and $a = 0.3$ for all drops.
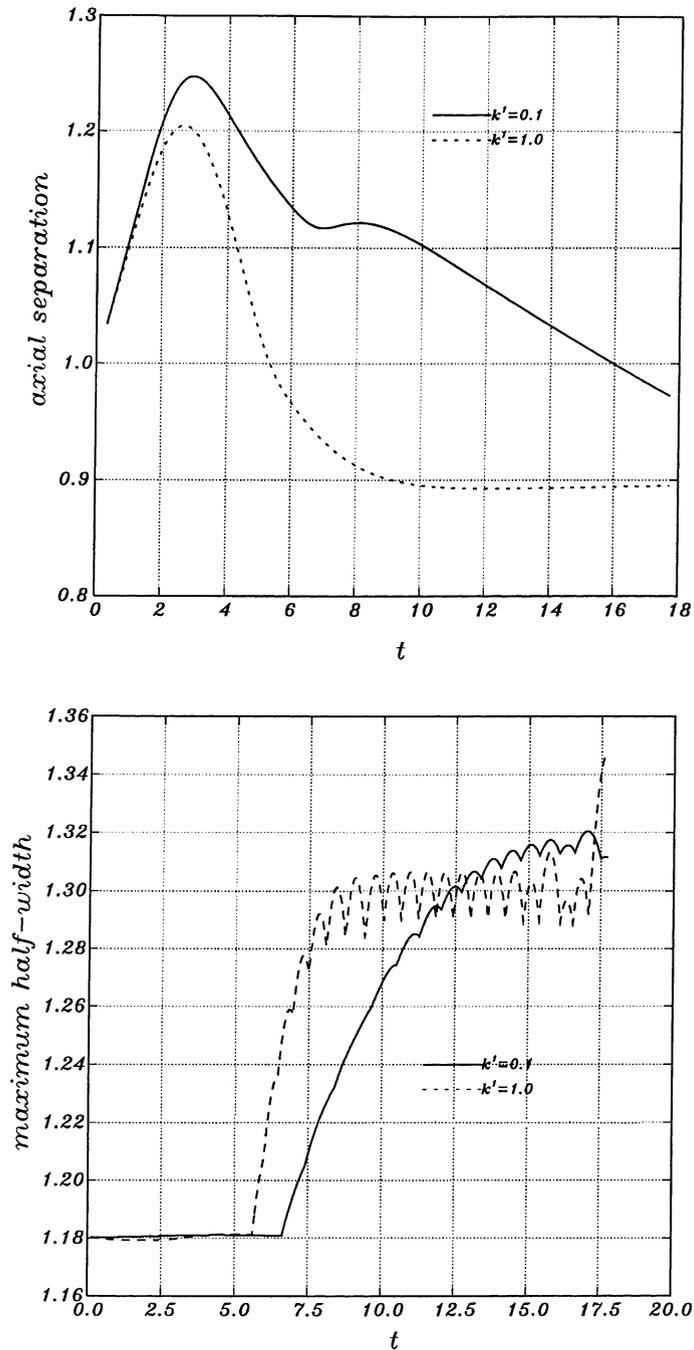
Fig. 9. (a) Axial separation between the front drop and those at the back from Figs. 7 and 8, and (b) maximum lateral extent of the jet.

As is evident from Eq. (2.12), the drop surface, in the case of a viscosity-matched drop, affects the dynamics through the third term in right-hand side. The integrand $k^{\alpha} \mathcal{C} n_i G(x, x_0)$ increases with k^{α}. The effect of the drop radius is felt through the curvature $\mathcal{C}$, as well as closeness to the jet surface, i.e. $|x - x_0|$ is small. The jet swelling is governed not by the magnitude, but by the *change* in this term as the drop moves and deforms. One can also think of the interfacial tension as a force opposing extension of the area (in this two-dimensional case, the circumscribing length) of a drop. Inside the nozzle, the drop is extended due to the flow working against the tension, which is relaxed in the jet, releasing the stored energy. A smaller drop would deform much less due to its larger stiffness, and therefore, would lead to a smaller effect.

Next, we consider three equal size drops of radius $a = 0.3$, placed initially in a triangular configuration (Fig. 7). Initial drop positions are $(-1.5, 0.0)$, $(-2.5, -0.4)$ and $(-2.5, 4.0)$. The computational domain is also increased to $L^{\text{in}} = 6$ and $L^{\text{out}} = 10$. For $k^1 = 0.1$, the drops show considerable deformation, especially those away from the center-line, and then they relax gradually, leading to further swelling of the jet. For an increased value of tension $k^1 = 1.0$, the deformation of the jet surface is predictably more, and the drops are observed to recover their circular shapes quickly (Fig. 8). Swelling can be augmented by drops coming together giving rise to a local inhomogeneity in the concentration. In Fig. 9(a), we plot the lateral separation between the front drop and those at the back. The drops are seen first to increase
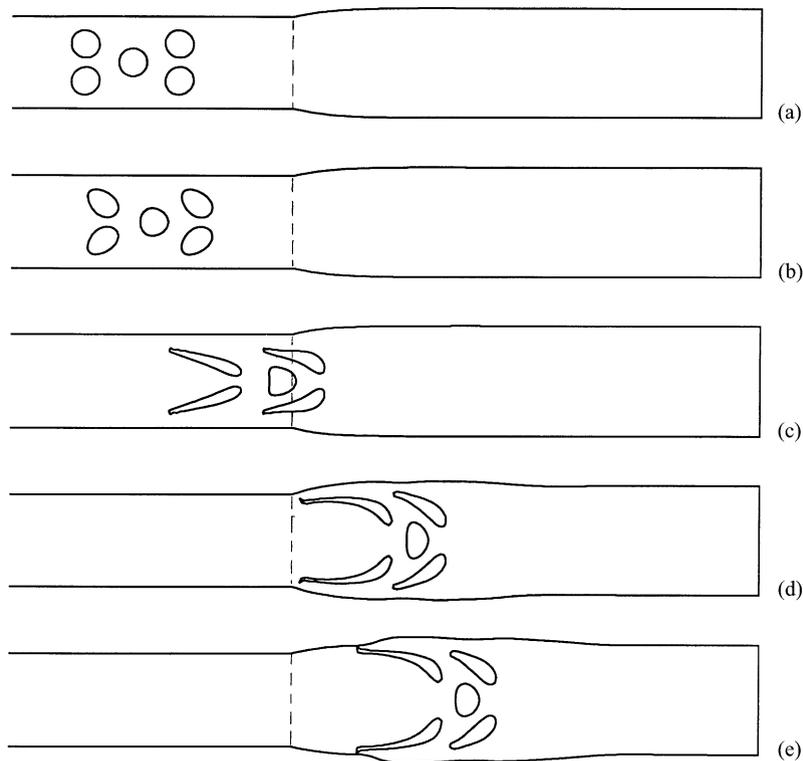
Fig. 10. Time-shots at (a) $t = 0.09$, (b) $t = 0.79$, (c) $t = 5.06$, (d) $t = 12.47$, (e) $t = 15.77$, for $k^1 = 0.1$ and $a = 0.3$ for all five drops.

separation due to the parabolic profile inside the jet, but then to come closer as they exit the nozzle. The change in slope for $k^1 = 0.1$ near $t = 7$ coincides with the elongated tails of the drops at the back coming out of the exit (see Fig. 7c). The $k^1 = 0.1$ case relaxes more slowly. Note that this case experiences large deformation (Fig. 7). On the other hand $k^1 = 1.0$ reaches a steady separation length, thereafter being convected by the plug flow. The maximum half-width of the jet as a function of time plotted in Fig. 9(b) shows the effect of the faster relaxation for the more elastic drop.

To investigate these effects further we present results for five equal size drops of radius $a = 0.3$, placed at $(-4.5, -0.4)$, $(-4.5, 0.4)$, $(3.5, 0.0)$, $(-2.5, -0.4)$ and $(-2.5, 0.4)$. The size of the computational domain is increased to $L^{\text{in}} = 6.0$, and $L^{\text{out}} = 10.0$. Figs. 10 and 11 show the evolution for $k^1 = 0.1$ and $k^1 = 1.0$, respectively. As before, the lower interfacial tension case gives rise to significantly more deformation. However, the effect on the jet surface is more in the other case. The drop configuration leads to a complex dynamics in this case. We have plotted the separations of the middle drop from those in the front as well as those in the back in Fig. 12. As can be seen, the drop in the middle catches up with those in the front within the nozzle due to convection. Again the one with $k^1 = 1.0$ reaches a steady state faster. The maximum half-width plotted in Fig. 13 shows that the jet with more elastic drops grows more quickly, but then attains a steady state, while the other slowly continues to grow, and may eventually reach a larger width.
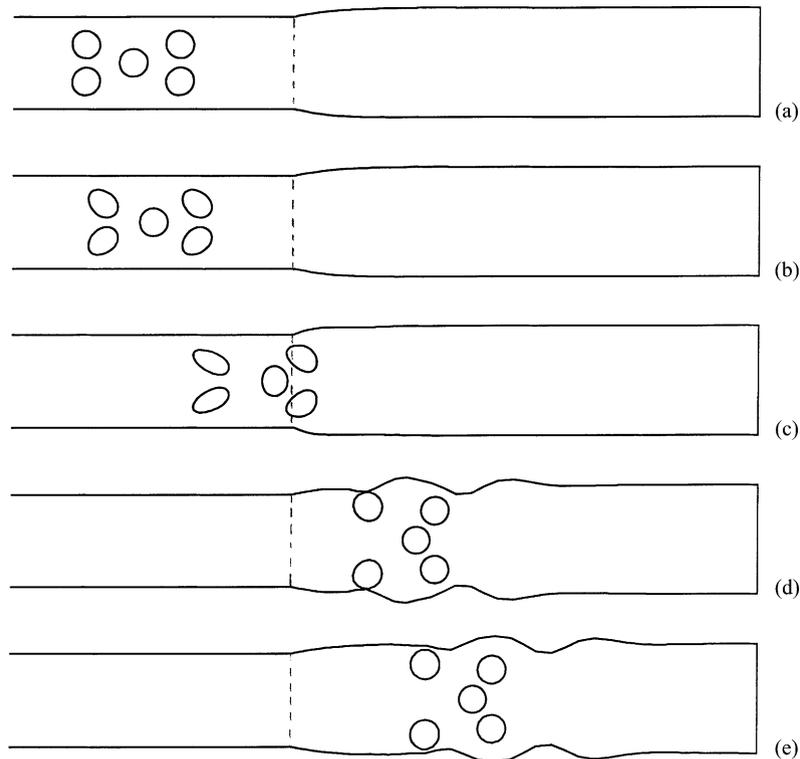
Fig. 11. Time-shots at (a) $t = 0.09$, (b) $t = 0.79$, (c) $t = 5.06$, (d) $t = 12.47$, (e) $t = 15.77$, for $k^1 = 1.0$ and $a = 0.3$ for all five drops.
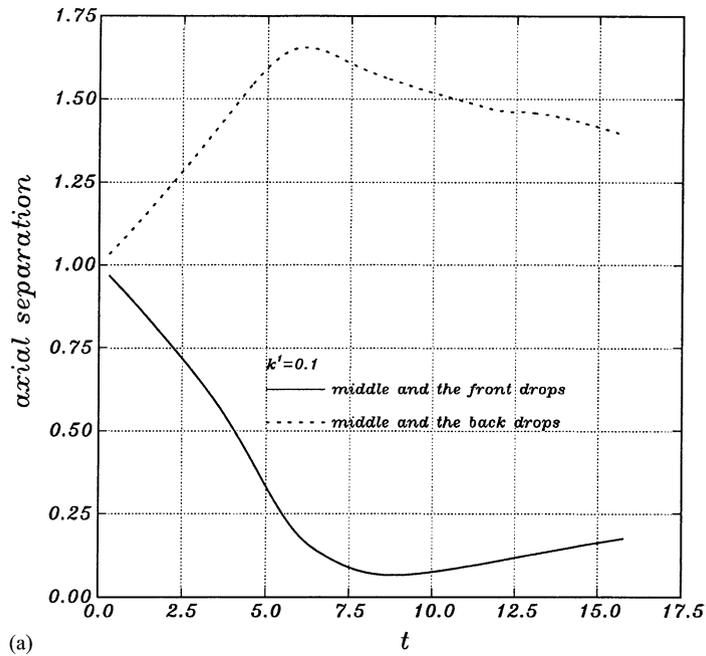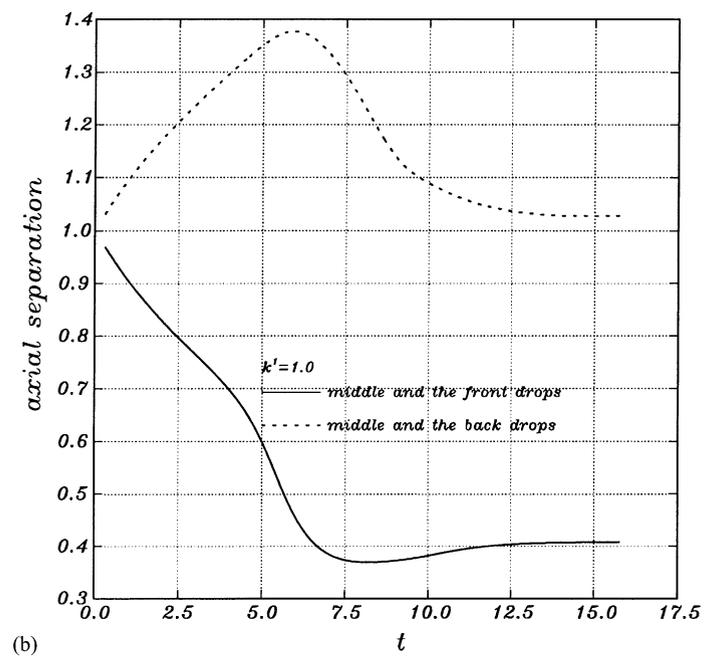
Fig. 12. Axial separations between the middle drop and those at the back and the front, for (a) $k^1 = 0.1$ (Fig. 10) and for (b) $k^1 = 1.0$ (Fig. 11).
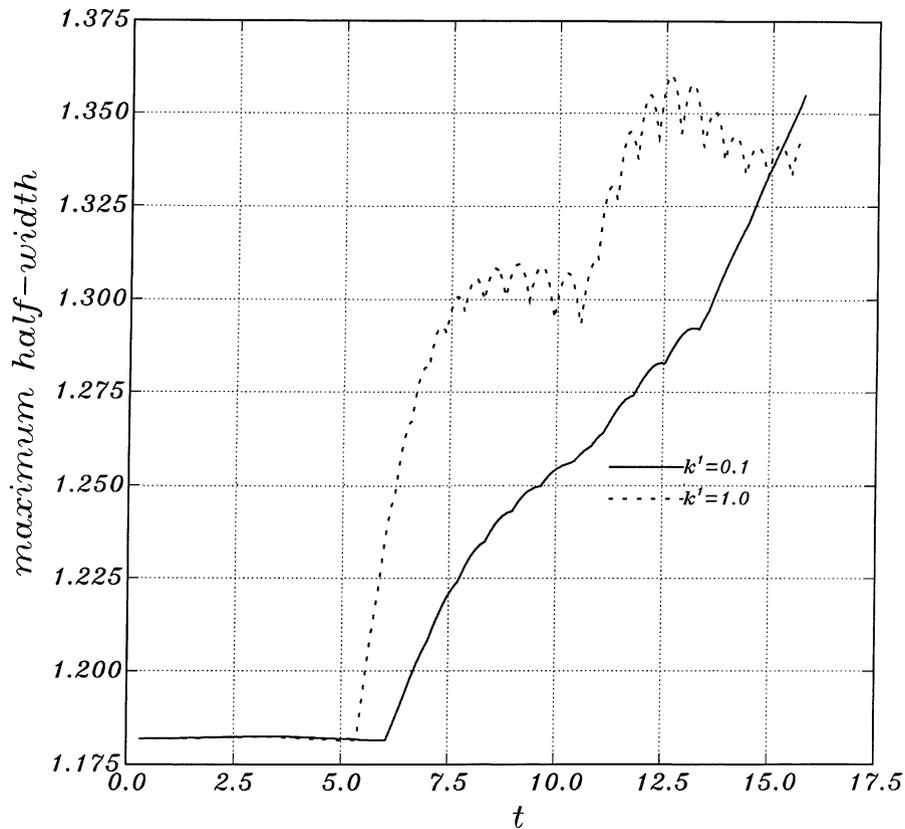
Fig. 13. Maximum lateral extent of the jet as a function of time for the five-drop cases (Figs. 10 and 11).

4. Summary

We have developed a model for a two-phase jet that follows the time history of the deformation and motion of individual drops. Our aim is to provide a detailed description of the non-Newtonian behavior of the jet resulting from interactions between drops and between the discontinuous and continuous phases. From the results one can infer the effect of recoil of the drops on the jet. Features of the model include artificial inlet and outlet boundaries, where the flows have been assumed to be parabolic and plug profiles, respectively. Neglecting the effects of gravity and inertia, we assumed Stokes flow in the domain occupied by the two phases. The boundary value problem is solved using the boundary element method in two dimensions. We investigated cases with one, three and five drops present in the jet. The drop motion is described for different values of drop radii, interfacial tensions and drop configurations. It is seen that the interacting drop dynamics presents an interesting time history marked by drop aggregation and relaxation of their deformation. Various parameters give rise to significant variation in the dynamics of the problem.

Finally, the present work with a few drops is a first step towards describing an emulsion jet. For a large industry scale process with numerous drops, the approach of course is prohibitively resource intensive, and therefore, at this point of time, unfeasible. However, the model problem has brought to fore some

important features of the actual phenomenon. Moreover, a microjet with sparsely embedded drops similar to the situation studied here has many potential applications in MEMs devices such as inkjets.

Appendix A

The expressions appearing in Eq. (2.15) are provided below:.

$$\overline{\mathcal{A}}_j^{r;\text{in}} = -\int_{\partial\Omega^{\text{in}}} G_{1j}(x, x_r)\,dl(x), \qquad \mathcal{A}_j^{r;\text{in}} = -\int_{\partial\Omega^{\text{in}}} 2x_2 G_{2j}(x, x_r)\,dl(x),$$

$$\mathcal{B}_{ij}^{r;\text{in}} = \int_{\partial\Omega^{\text{in}}} (1 - x_2^2) T_{ijk}(x, x_r) n_k(x)\,dl(x), \tag{A.1}$$

$$\mathcal{A}_{ij}^{rs} = \int_{\partial\Delta^s} G_{ij}(x, x_r)\,dl(x), \qquad \mathcal{B}_{ij}^{rs} = \int_{\partial\Delta^s} T_{ijk}(x, x_r) n_k(x)\,dl(x), \tag{A.2}$$

$$\mathcal{A}_j^{r;\text{free}} = \int_{\partial\Omega^f} G_{ij}(x, x_r)\mathcal{C}(x) n_i(x)\,dl(x), \qquad \mathcal{A}_j^{r;\alpha} = \int_{\partial\Omega^\alpha} G_{ij}(x, x_r)\mathcal{C}(x) n_i(x)\,dl(x). \tag{A.3}$$

Δ^s is the s-th element on the discretized surface. The last expressions are computed by integrating over smaller elements over the free surface and the drops and summing them.

Appendix B

As is evident from the Eq. (2.10) $G_{ij}(x, x_0)$ and $T_{ijk}(x, x_0)$ are singular in the limit $x_0 \to x$, hence special attention is required while performing the integrals ([23,pp. 177–180]). In this implementation, only when x_0 is in the same element as x, have we resorted to a special treatment. For $\mathcal{A}$ terms involving G_{ij}, even though it has an integrable singularity, we subtract the logarithm term from G_{ij} in Eq. (2.10), and express its integral over the element (l_a, l_b) as follows:

$$\int_{l_a}^{l_b} \ln|x - x_0|\,dl(x) = (l_0 - l_a)\ln|x_a - x_0| + (l_b - l_0)\ln|x_b - x_0| - (l_b - l_a). \tag{B.1}$$

For $\mathcal{B}$ integrals involving T_{ijk}, we remove the singular element contribution to get the principal value.

References

[1] S. Middleman, J. Gavis, Expansion and contraction of capillary jets of Newtonian liquids, Phys. Fluids 4 (1961) 355, errat: 4 (1961) 1450.

[2] S.L. Goren, S. Wronski, The shape of low-speed capillary jets of Newtonian liquids, J. Fluid Mech. 25 (1966) 185.
[3] S. Richardson, The die-swell phenomenon, Rheol. Acta 9 (1970) 193.
[4] S. Richardson, A stick-slip problem related to the motion of a free jet at low Reynolds numbers, Proc. Cambridge Phil. Soc. 67 (1970) 477.
[5] S.A. Trogdon, D.D. Joseph, The stick-slip problem for a round jet. I. Large surface tension, Rheol. Acta 19 (1980) 404.
[6] S.A. Trogdon, D.D. Joseph, The stick-slip problem for a round jet. II. Small surface tension, Rheol. Acta 20 (1981) 1.
[7] L.D. Sturges, A theoretical study of extrudate swell, J. Non-Newtonian Fluid Mech. 9 (1981) 357.
[8] R.E. Nickell, R.I. Tanner, B. Caswell, The solution of viscous incompressible jet and free-surface flows using finite element methods, J. Fluid Mech. 65 (1974) 189.
[9] M.J. Crochet, R. Keunings, Die swell of Maxwell fluids: numerical prediction, J. Non-Newtonian Fluid Mech. 7 (1980) 199.
[10] M.B. Bush, R.I. Tanner, Numerical solution of viscous flows using integral equation methods, Int. J. Num. Meth. Fluids 3 (1983) 71.
[11] H.A. Tieu, D.D. Joseph, Extrudate swell for a round jet with large surface tension, J. Non-Newtonian Fluid Mech. 13 (1983) 203.
[12] M.B. Bush, J.F. Milthrope, R.I. Tanner, Finite element and boundary element methods for extrusion computations, J. Non-Newtonian Fluid Mech. 16 (1984) 37.
[13] M.B. Bush, R.I. Tanner, N. Phan-thien, A boundary element investigation of extrudate swell, J. Non-Newtonian Fluid Mech. 18 (1985) 143.
[14] G.C. Georgiou, W.W. Schultz, L.G. Olson, Singular finite elements for the sudden expansion and the die-swell problems, Int. J. Num. Meth. Fluids 10 (1990) 357.
[15] T.R. Salamon, D.E. Bornside, R.C. Armstrong, R.A. Brown, The role of surface tension in the dominant balance in the die swell singularity, Phys. Fluids 7 (1995) 2328.
[16] E. Mitsoulis, Three-dimensional non-Newtonian computations of extrudate swell with the finite element methods, Comput. Meth. Appl. Mech. Engr. 180 (1999) 333.
[17] H. Ouddiz, Epaississement des jets d'emulsions modele huile de silicone/EAU, DEA mecanique Paris VI/ENSTA, Ecole Nationale Superieure de Techniques Avancees, Juin, 1988.
[18] D. Fruman, P. Perrot, J. Bouguechal, On the swelling of submerged jets of dilute and semi-dilute polymer solutions, Chem. Eng. Commun. 27 (1984) 101.
[19] G.K. Batchelor, The stress system in a suspension of force-free particles, J. Fluid Mech. 41 (1970) 545.
[20] W.J. Silliman, L.E. Scriven, Separating flow near a static contact line: slip at a wall and shape of a free surface, J. Comput. Phys. 34 (1980) 287.
[21] G.K. Youngren, A. Acrivos, Stokes flow past a particle of arbitrary shape: a numerical method of solution, J. Fluid Mech. 69 (1975) 377.
[22] G.K. Youngren, A. Acrivos, On the shape of a gas bubble in a viscous extensional flow, J. Fluid Mech. 76 (1976) 433.
[23] C. Pozrikidis, Boundary Integral and Singularity Methods for Linearized Viscous Flow, Cambridge University Press, Cambridge, 1992.
[24] M. Loewenberg, E.J. Hinch, Numerical simulation of a concentrated emulsion in shear flow, J. Fluid Mech. 321 (1995) 395.
[25] M. Manga, Dynamics of drops in cavity flows: aggregation of high viscosity ratio drops, Phys. Fluids 8 (1996) 1732.
[26] S.O. Unverdi, G. Tryggvason, A front-tracking method for viscous, incompressible multi-fluid flows, J. Comp. Phys. 100 (1988) 25.
[27] A. Esmaeeli, G. Tryggvason, Direct numerical simulations of bubbly flows. Part 1. Low Reynolds number arrays, J. Fluid Mech. 377 (1998) 313.
[28] A. Esmaeeli, G. Tryggvason, Direct numerical simulations of bubbly flows. Part 2. Moderate Reynolds number arrays, J. Fluid Mech. 385 (1999) 325.